A facile route for preparing rhabdophane rare earth phosphate nanorods

Xiaojuan Wang and Mingyuan Gao*

Received 5th December 2005, Accepted 6th January 2006
First published as an Advance Article on the web 23rd January 2006
DOI: 10.1039/b517179b

Lanthanum orthophosphate nanorods with typical dimensions of 8 nm in diameter and 80 nm in length were prepared simply by mixing NaH_2PO_4 and $LaCl_3$ aqueous solutions in an oil bath of 100 °C. Eu^{3+}- and Ce^{3+}-doped nanorods were also be prepared in a similar way by introducing Eu^{3+} and Ce^{3+} ions, respectively, into the reaction systems. TEM (transmission electron microscope) and XRD (X-ray diffraction) results revealed that the above-mentioned lanthanide orthophosphate nanorods possessed a rhabdophane-type structure. Compositional analysis by X-ray photoelectron spectroscopy demonstrated that $LaPO_4$ nanorods had an anion-rich surface, which might be the main reason for their colloidal stabilities. The appearance of radiating aggregates during the early stage of the precipitation reactions and their pH dependent morphologies indicated that the formation of lanthanide orthophosphate nanorods was mainly governed by the growth nature of hexagonal $LaPO_4$. The optical measurements indicated that $LaPO_4 : Ce^{3+}$ with the rhabdophane structure has stronger electron–phonon coupling than monazite-type. The fluorescence quantum yield of $LaPO_4 : Ce^{3+}$ nanorods was estimated to be 35%. In comparison with rhabdophane nanoparticles, the strongest emission of the Eu^{3+}-doped nanorods originates from the $^5D_0$ to $^7F_1$ transition rather than $^5D_0$ to $^7F_2$. This may be attributed to the nature of the 1D structure as well as the lattice distortions in the nanorods.

Introduction

It is well known that both size and dimensions are very important parameters determining the properties of a nanomaterial.[1,2] With reduced dimensions and size, one-dimensional nanomaterials such as nanorods, nanowires, nanotubes and nanobelts present unique optical, thermal, electronic, mechanical, magnetic and electron-transport properties.[3,4] For example, by the taking advantage of low melting temperatures functional devices and circuitry are hopefully formed by cutting, linking and welding the 1D nanowires;[5] well-monodispersed CdSe nanorods however are expected to be useful as polarized light emitting diodes, flat panel displays, and electrooptic modulators due to their ability to form liquid crystal phases in organic solvents;[6] ZnO nanowires not only present ultra-high field emission due to their high aspect ratio,[7] but also show lasing action and photoconductivity, which make them useful candidates for field-emission devices, laser, and optoelectronic switches.[8,9]

Different from II–VI semiconductor, metal and metal oxides, rare-earth compounds such as lanthanides present quite unique optical properties because their electronic structures and numerous transition modes involving the 4f electrons are not susceptible to the environment under the shield of the outer shell electrons. In addition, the optical properties of lanthanide doped materials are normally characterized by narrow emissions and large Stokes shifts, which make the rare-earth compounds excellent phosphors.[10] Some lanthanide compounds can also be used as effective catalysts[11,12] or magnetically functional host materials.[13] Recent developments further demonstrated that nanocrystals of rare-earth compounds exhibit great potential in medical imaging as an alternative to quantum dots.[14,15]

Lanthanide orthophosphates, as an important family member of the rare-earth compounds, have attracted increasing attention due to their special physical and chemical properties. To reduce the size and dimensions of lanthanide orthophosphates will no doubt lead to new physical and chemical properties. For instance, Eu^{3+}-doped $LaPO_4$ nanowires have shown the highest fluorescence quantum yield and improved radiative transition rate in comparison with their corresponding nanoparticles, microparticles and microrods;[16] $CePO_4$ nanowires however exhibit two sharp emissions in the UV regime which are noticeably different from the bulk.[17] Up to now, most lanthanide phosphate nanomaterials with various 1D structures, such as nanorods, nanowires and nanocables, are prepared by hydrothermal or modified hydrothermal methods such as the hydrothermal microemulsion method and polymer-assisted hydrothermal methods.[18–23] However, to monitor the reactions taking place under extreme conditions in an autoclave is practically difficult and inconvenient. In this paper, we report a facile synthetic route for preparing $LaPO_4$, Ce^{3+}- and Eu^{3+}-doped $LaPO_4$ nanorods under very mild conditions by a wet-chemical method. The possible mechanism leading to $LaPO_4$ nanorods was investigated. The optical properties of the nanorods are also discussed herein.

Key Laboratory of Colloid, Interface Science and Chemical Thermodynamics, Institute of Chemistry, CAS, Zhong Guan Cun, Bei Yi Jie 2, Beijing, 100080, China. E-mail: gaomy@iccas.ac.cn; Fax: 0086 10 8261 3214

Experimental

$LaCl_3 \cdot 7H_2O$, $CeCl_3 \cdot 6H_2O$ and $EuCl_3 \cdot 6H_2O$ used in the syntheses of lanthanide phosphate were commercially available products with purities of 99.99%. $NaH_2PO_4 \cdot 2H_2O$ used was of A.R. grade. First, 10 mL aqueous solution of 0.1 M NaH_2PO_4 and 10 mL aqueous solution of 0.1 M $LaCl_3 \cdot 7H_2O$ were prepared separately. Then, they were mixed and subjected to an oil bath of 100 °C. After being maintained in the oil bath for a certain period of time, the reaction mixture was cooled to room temperature. Upon addition of acetone, white precipitates appeared and were collected by centrifugation at 4000 rpm for 5 min. The purification of the white precipitates was done by re-dispersing them in deionized water followed by addition of acetone, and collection by centrifugation for 5 cycles.

$LaPO_4 : Ce^{3+}$ and $LaPO_4 : Eu^{3+}$ nanorods were prepared in a similar way. The typical feed molar ratios of Ce : La and Eu : La were 1 : 2 and 1 : 9, respectively. The doped $LaPO_4$ samples obtained were purified by dialysis against deionized water for 2 days.

Powder X-ray diffraction (XRD) patterns were taken with a Rigaku D/Max-2500 diffractometer using a Cu target radiation source (Cu Kα = 1.54078 Å). Fourier transform infrared spectroscopy (FTIR) analysis was performed with a Bruker EQUINOX55 infrared spectrometer on KBr pellets in the region of 400–4000 cm^{-1} with 4 cm^{-1} resolution under ambient conditions. Transmission electron microscopy (TEM) images were captured on a JEM-100CXII electron microscope operating under an acceleration voltage of 100 kV. A high-resolution TEM (HTEM) image was taken on a JEM-2010 electron microscope under an acceleration voltage of 200 kV. X-Ray photoelectron spectroscopy (XPS) measurements were performed on a VG ESCALAB 220i-XL spectrometer. All binding energies for different elements were calibrated with respect to the C1s line at 284.6 eV for the contaminant carbon. A combination of a Shirley-type background and a linear-type background was used for curve-fitting. A Cary 50 UV-Visible spectrophotometer and a Cary Eclipse spectrophotometer were used in the optical characterizations.

The fluorescence quantum yield (QY) of the $LaPO_4 : Ce^{3+}$ nanorods was estimated by using Rhodamine 6G (R6G) as a fluorescence standard. A fluorescence efficiency of 95% was taken for R6G in diluted ethanol solution according to reference 24. The fluorescence quantum yield of the Ce^{3+}-doped $LaPO_4$ nanorods was estimated to be 35%.

Results and discussion

Three representative TEM images of undoped, and Ce^{3+}- and Eu^{3+}-doped $LaPO_4$ samples are shown in Fig. 1. The average diameter of the undoped $LaPO_4$ nanorods is 7.8 nm, while the average length is 82.0 nm. Compared with the undoped $LaPO_4$ nanorods, the Ce^{3+}- and Eu^{3+}-doped nanorods show little differences in both rod length and diameter as shown in Table 1. Under high resolution TEM, the $LaPO_4$ nanorods appear as single crystals with a *d*-spacing between two adjacent lattice planes parallel to the long axis of 6.15 Å, which is in good agreement with the theoretical interplanar spacing

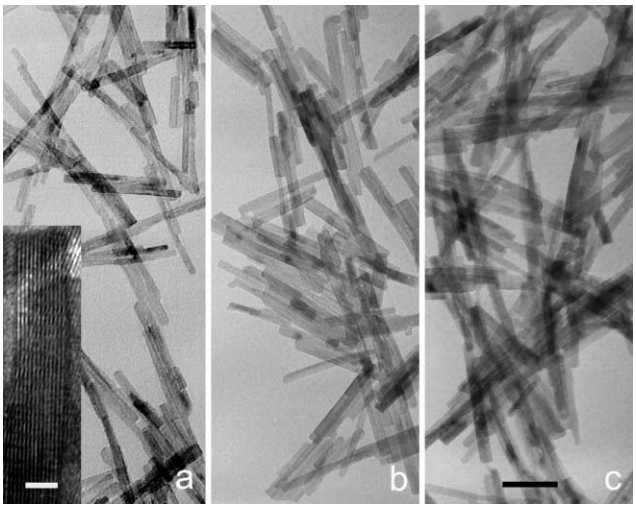

Fig. 1 Representative TEM images of $LaPO_4$ (a), $LaPO_4 : Ce^{3+}$ (b) and $LaPO_4 : Eu^{3+}$ nanorods (c). The scale bar corresponds to 50 nm. Inset: A high-resolution TEM (HRTEM) image of $LaPO_4$ nanorods. The scale bar corresponds to 5 nm.

Table 1 Summary of statistical dimensions of undoped and doped $LaPO_4$ nanorods

Nanorods	$LaPO_4$	$LaPO_4 : Ce^{3+}$	$LaPO_4 : Eu^{3+}$
Diameter/nm	7.8 ± 1.9	8.0 ± 1.9	8.3 ± 1.7
Length/nm	82.0 ± 24.3	76.3 ± 27.6	79.3 ± 26.8
Aspect ratio/nm	10.9 ± 3.6	9.7 ± 3.1	9.7 ± 3.2

(6.11 Å) for (100) planes of hexagonal rhabdophane $LaPO_4$. This demonstrates that the $LaPO_4$ nanorods occur in a hexagonal structure and grow along the *c* axis, *i.e.*, the [100] direction. In some cases, bent lattice fringes also appear, indicating that there is some lattice distortion in the nanorods.

The crystalline structure of those samples shown in Fig. 1 was further identified by X-ray powder diffraction. The XRD patterns shown in Fig. 2 demonstrate that both doped and undoped nanorods are hexagonal rhabdophane $LaPO_4$ according to standard atomic spacing for $LaPO_4 \cdot 0.5H_2O$ (JCPDS card: 46-1439). In comparison with the standard diffraction pattern, in the inspected range from 10° to 80°, no

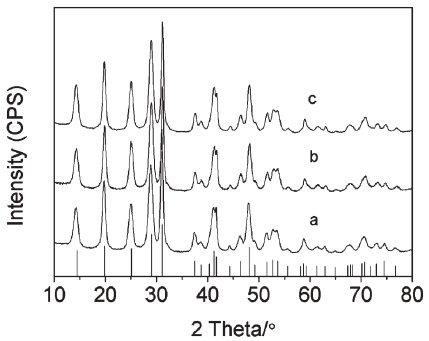

Fig. 2 XRD patterns of the nanorods shown in Fig. 1: $LaPO_4$ (a); $LaPO_4 : Ce^{3+}$ (b) and $LaPO_4 : Eu^{3+}$ (c). The standard diffraction lines of hexagonal $LaPO_4 \cdot 0.5H_2O$ (JCPDS card: 46-1439) are also shown at the bottom.

diffraction peaks from $CePO_4$ or $EuPO_4$, which may exist as impurities, are observed from the doped samples. Furthermore, most of the diffraction peaks from doped $LaPO_4$ slightly shift to higher angle in comparison with those for the undoped $LaPO_4$, suggesting that Ce^{3+} or Eu^{3+} ions are doped into the $LaPO_4$ matrix because both $CePO_4$ and $EuPO_4$ possess smaller *d*-spacings than $LaPO_4$. In addition, by Sherrer's formula, the particle sizes derived from the (100) peaks of $LaPO_4$, $LaPO_4 : Ce^{3+}$ and $LaPO_4 : Eu^{3+}$ are calculated to be 8.1, 8.4 and 8.4 nm, respectively, roughly in agreement with the diameters obtained by TEM, which indicates that the nanorods possess nearly single crystal structures.

The $LaPO_4$ nanorods were also characterized by Fourier transform infrared (FTIR) spectroscopy. The FTIR results indicate that the PO_4^{3-} groups occur in discrete states, while zeolitic water molecules exist in the channel-type structure of $LaPO_4$,[25,26] which is in agreement with the hexagonal rhabdophane $LaPO_4$ structure identified by XRD.

X-Ray photoelectron spectroscopy was adopted to investigate the binding situations of La, P and O in the $LaPO_4$ nanorods obtained. Fig. 3 exhibits a binding energy survey from 0 to 1200 eV. The peaks locating at 835.5 eV, 132.7 eV, and 531.2 eV can be assigned to the binding energies of $La3d_{5/2}$, P2p, and O1s in $LaPO_4$ nanorods, respectively.[27] The XPS spectrum in the range of 186 to 203 eV, where the binding energies of La and P are located, was carefully fitted. It turns out that phosphorus overwhelmingly exists in the form of PO_4^{3-} groups according to its binding energy of P2s located at

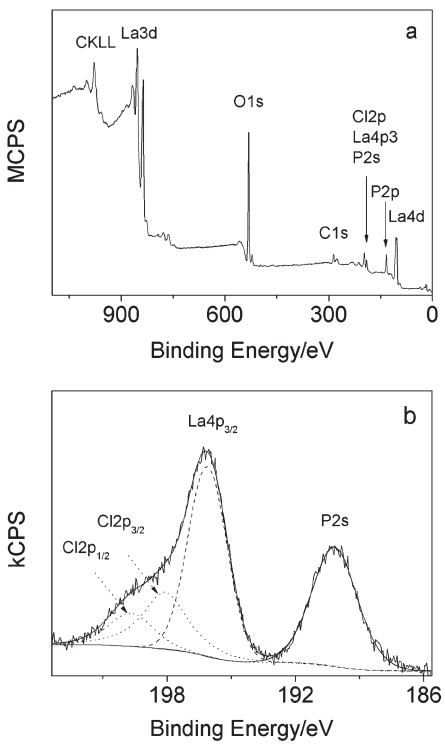

Fig. 3 X-Ray photoelectron spectrum of undoped $LaPO_4$ nanorods (a) and an enlarged part of the same spectrum where binding energies of $La4p_{3/2}$, Cl2p and P2s are located together with the corresponding fitted curves.

190.2 eV. Unexpectedly, two additional peaks appear at 198.1 eV and 199.7 eV, split by 1.6 eV. These two peaks can be assigned to $Cl2p_{3/2}$ and $Cl2p_{1/2}$ orbitals, respectively.[28] Nonetheless, within the whole energy regime, no Na1s orbital emission appears at all, excluding the existence of chlorine from NaCl impurity. The resultant atomic ratio of La : P : Cl is calculated to be 1 : 1.5 : 0.24. The existence of excess phosphorus and chlorine implies that the surface of $LaPO_4$ nanorods is occupied by anions, which explains their good aqueous colloidal stability since electrostatic repulsions dominate the interactions among nanorods.

In comparison with most synthetic routes for 1D lanthanide phosphates, the current approach is characterized by very mild preparation conditions. Therefore, it is necessary to understand the formation mechanism for lanthanide phosphate nanorods. In fact, there exist some reports on nanometer sized rods and wires of lanthanide phosphate prepared in a liquid medium free of surfactant.[18–21] The anisotropic growth is generally interpreted by the chemical potentials of specific lattice planes and the mother solution which are determined by the concentration of monomers and features of crystal structures.[19,20,29] In the current case, the lanthanide phosphate nanorods obtained, as demonstrated by XRD, are of hexagonal structure, which is expected since the hexagonal structure is the only stable phase at low temperature for light rare earth phosphates. Since no surface stabilizing agents were used in the preparation, it can be deduced that the formation of 1D $LaPO_4$ is mainly determined by its own growth nature. It is known from the hexagonal crystal structure that anions and cations are placed alternately along the [001] direction, which gives rise to the largest amount of net charges and the strongest polarity for the (001) and (00$\underline{1}$) facets in comparison with other lattice planes. In the specific case of hexagonal lanthanum phosphate, most dangling bonds also concentrate on these two facets since two La–O bonds form a bridge between one La atom and one PO_4^{3-} tetrahedron along the [001] direction, while only one La–O bond binds with a PO_4^{3-} tetrahedron along other directions in the $LaPO_4$ crystal lattice. Therefore, the cooperation of electrostatic interactions with the dangling bond may mainly be responsible for the anisotropic growth since most counterions are readily attracted to the (001) and (00$\underline{1}$) facets to react.

According to this interpretation, an increased aspect ratio can reasonably be expected by raising the pH of the reaction system since the electrostatic interactions between either the (001) or (00$\underline{1}$) facet and the counterions in the solution will be enhanced due to the deprotonation of PO_4^{3-} while the electrostatic interactions on the surface parallel to the [001] direction are reduced due to the decline of net charges. To verify this, two additional lanthanum phosphate nanorod samples were prepared by mixing NaH_2PO_4 solutions of pH 1.2 and 6.9 with two identical $LaCl_3$ aqueous solutions (the original pH of 0.1 M NaH_2PO_4 is 4.4). TEM results shown in Fig. 4 reveal that the $LaPO_4$ nanorods obtained at lower pH clearly exhibit a smaller aspect ratio than those obtained at higher pH. This is in agreement with the observation by Fang *et al.* on hexagonally structured lanthanide phosphate nanowires[19] and further confirms the above-proposed growth mechanism. Meanwhile, this mechanism can explain why the

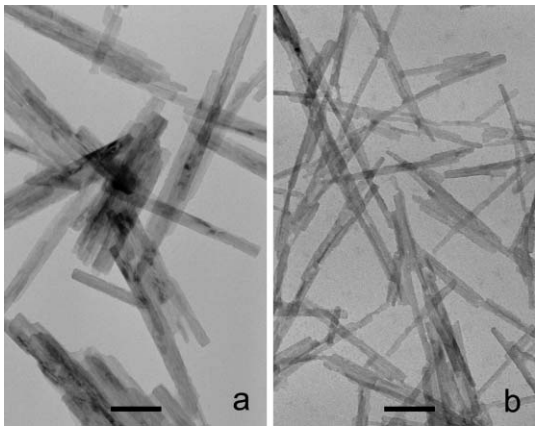

Fig. 4 TEM images of $LaPO_4$ nanorods prepared by mixing NaH_2PO_4 solutions of pH 1.2 (a) and 6.9 (b) with two identical $LaCl_3$ aqueous solutions. The scale bars correspond to 50 nm.

reverse variation of morphology with pH value is observed in the monoclinic structure.

The morphological changes in $LaPO_4$ nanostructures formed during the early stage of the reaction also support the aforementioned growth mechanism. It was observed that a large percentage of radiating aggregates composed of nanorods were initially formed right after the two reactant solutions were mixed, as shown in Fig. 5. The rapid formation of a quasi-1D substructure can be attributed to the choice of precursors since they possess excellent aqueous solubility which promises the highest available concentrations of monomers and favors anisotropic growth. Compared with the as-mixed sample formed at room temperature (Fig. 5b), the sample formed at elevated temperature (Fig. 5a) possesses better defined rod morphologies in substructures. This may be associated with the temperature-dependent pH effect as well as the temperature-dependent growth kinetics. The following observations revealed that the radiating aggregates were completely destroyed after being maintained in the oil bath of 100 °C for 1 minute, and subsequently formed separated nanorods. Due to the quick structural transformation, it was practically difficult to grasp more intermediate states. Nonetheless such a quick structural transformation proves that the rod structure is the most favorable structure for nanometer sized $LaPO_4$. The final formation of separated nanorods can be interpreted as follows. During the early stage of reaction, a large number of nuclei formed and aggregated. Meanwhile, 1D structures stemming from these nuclei quickly developed and formed radiating aggregates of nanorods. During the following growth stage, due to the fast growth at both ends of the 1D structures, the diffusion of monomers from surrounding media to aggregates may not be quick enough to compensate the monomer consumption at the inner part of aggregates. The growth of 1D structure along the direction pointing to the inner part of the aggregates has to be at the cost of the dissolution of the nuclei. As a result, the radiating aggregates quickly collapsed and formed separated nanorods.

Since rare-earth compounds are one of the most important types of phosphors, the optical properties of the doped nanorods were also investigated. In the absorption spectrum

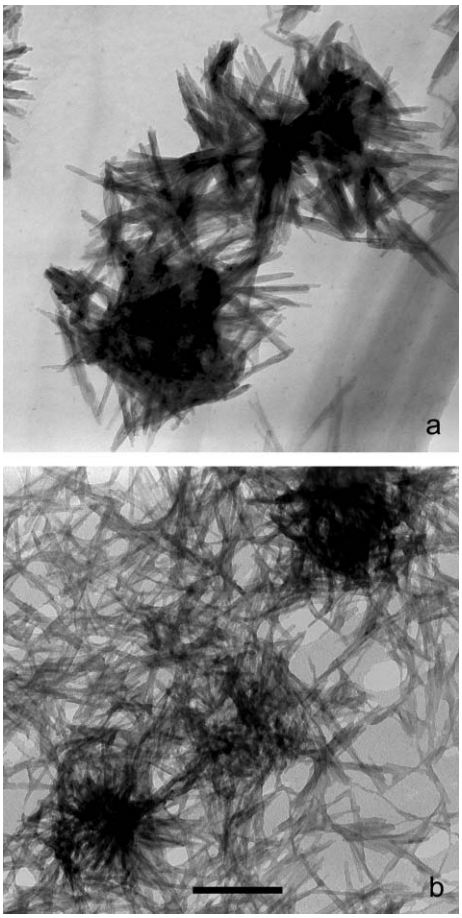

Fig. 5 The morphologies of as-mixed $LaPO_4$ nanorods formed in an oil bath of 100 °C (a) and at room temperature (b). The scale bar corresponds to 100 nm.

of $LaPO_4 : Ce^{3+}$ nanorods shown in Fig. 6, two absorption bands at 273 and 232 nm, together with an absorption shoulder at around 259 nm, can be resolved and assigned to transitions from the 4f ground state to the 5d energy levels split by the crystal field. Under UV irradiation at 270 nm, the $LaPO_4 : Ce^{3+}$ nanorods present a broad emission due to the 5d–4f transitions. The fluorescence quantum yield of this emission is estimated to be 35%. In fact, the broad emission is composed of two overlapped emissions according to the

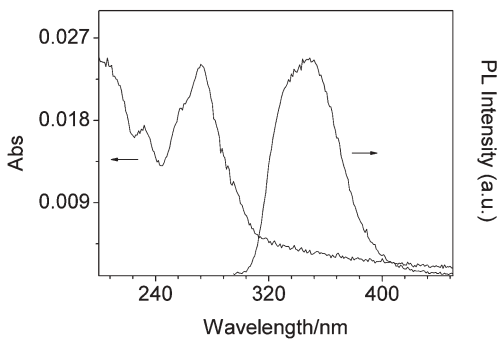

Fig. 6 Absorption and fluorescence spectra of $LaPO_4 : Ce^{3+}$ nanorods. The fluorescence spectrum was recorded by exciting the sample at 270 nm.

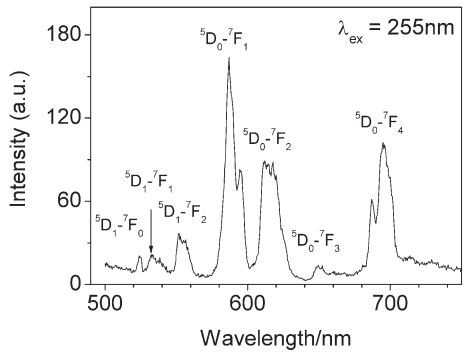

Fig. 7 Fluorescence spectrum of $LaPO_4 : Eu^{3+}$ nanorods recorded by exciting the sample at 255 nm.

literature,[30] resembling the emissions of bulk $CePO_4$ recorded at −180 °C.[31] These two emission bands can be assigned to transitions from the 5d excited state to two split 4f ground states, $^2F_{7/2}$ and $^2F_{5/2}$. Compared with monazite $LaPO_4 : Ce^{3+}$ nanowires reported by Yu *et al.*,[32] the luminescence of $LaPO_4 : Ce^{3+}$ nanorods presents an inconspicuous splitting between the ^2D–$^2F_{7/2}$ and ^2D–$^2F_{5/2}$ transitions, as well as a larger Stokes shift of about 30 nm, similar to hexagonal $LaPO_4 : Ce^{3+}$ nanoparticles.[33] These differences indicated that 5d electron of Ce^{3+} coupled more strongly to the crystal phonon in a hexagonal matrix than in a monoclinic matrix.[30] These results are similar to those reported by Brown *et al.*[34]

Compared with nanowires and nanoparticles, the 10% europium-doped $LaPO_4$ nanorods exhibit different optical properties.[19,33] Under excitation at 255 nm, as shown in Fig. 7, radiative emissions of $^5D_1$ to $^7F_0$, $^7F_1$ and $^7F_2$ transitions are presented in addition to those of $^5D_0$ to ^7F_J (J = 1–4). The former emissions were not observed by Fang *et al.* from $LaPO_4 : Eu^{3+}$ nanowires probably because the energy gap between the $^5D_1$ and $^5D_0$ levels in Eu^{3+} is bridged by the multiphoton relaxation based on the vibration of phosphate groups.[19] In contrast, the vibrational absorption of phosphate groups at 1053 cm^{-1} is much weaker with respect to the current $LaPO_4 : Eu^{3+}$ nanorods, which explains the appearance of radiative emissions from $^5D_1$ to $^7F_0$, $^7F_1$ and $^7F_2$. Moreover, the nanorods also present a different $^5D_0$–$^7F_4$ emission profile. The strongest line of the $^5D_0$–$^7F_4$ transitions is located at 695 nm rather than 687 nm. These different radiative transition behaviors may come from the differences in the crystal field at each lattice site as well as the energy transfer rate constant between adjacent sites, since these two parameters determine the transition probabilities from the $^5D_0$ state to the sublevels of the ^7F_J states.[18,35] In comparison with rhabdophane-type nanoparticles,[33] the strongest emission originates from the transition of $^5D_0$ to $^7F_1$ rather than $^5D_0$ to $^7F_2$. This may be due to the nature of the 1D structure and the existence of lattice distortions in the matrix of $LaPO_4 : Eu^{3+}$ nanorods since $^5D_0$ to $^7F_2$ transitions are hypersensitive to the symmetry of the crystal field.

Conclusions

Doped and undoped hexagonal lanthanide orthophosphate nanorods have been synthesized in aqueous solution by using NaH_2PO_4 and $LaCl_3$ as precursors. The good aqueous solubility of these two precursors enables a very quick precipitation reaction which generates nanorods under very mild conditions. Detailed investigations reveal that the unique crystalline features of the hexagonal $LaPO_4$ play a determined role in the formation of the 1D nanostructure. Optical characterizations reveal that the Ce^{3+}-doped lanthanum orthophosphate nanorods possess a broad photoluminescence between 300 and 400 nm with the fluorescence quantum yield being up to 35%. The Eu^{3+}-doped lanthanum orthophosphate nanorods show different luminescence properties in comparison with the corresponding nanowires or nanoparticles. In conclusion, the current investigations demonstrate that hexagonally structured lanthanide orthophosphate nanorods can be prepared under very mild conditions, which may provide valuable instructions for facile preparations of other types of doped or undoped 1D rare-earth nanomaterials.

References

1 C. J. Murphy and N. R. Jana, *Adv. Mater.*, 2002, **14**, 80.
2 S. Kan, T. Mokari, E. Rothenberg and U. Banin, *Nat. Mater.*, 2003, **2**, 155.
3 Y. Xia, P. Yang, Y. Sun, Y. Wu, B. Mayers, B. Gates, Y. Yin, F. Kim and H. Yan, *Adv. Mater.*, 2003, **15**, 353.
4 D. H. Reich, M. Tanase, A. Hultgren, L. A. Bauer, C. S. Chen and G. J. Meyer, *J. Appl. Phys.*, 2003, **93**, 7275.
5 Y. Wu and P. Yang, *Adv. Mater.*, 2001, **13**, 520.
6 L. Li, J. Walda, L. Manna and A. P. Alivisatos, *Nano Lett.*, 2002, **2**, 557.
7 D. Banerjee, S. H. Jo and Z. F. Ren, *Adv. Mater.*, 2004, **16**, 2028.
8 M. H. Huang, S. Mao, H. Feick, H. Yan, Y. Wu, H. Kind, E. Wever, R. Russo and P. Yang, *Science*, 2001, **292**, 1897.
9 H. Kind, H. Yan, B. Messer, M. Law and P. Yang, *Adv. Mater.*, 2002, **14**, 158.
10 C. Feldmann, T. Jüstel, C. R. Ronda and P. J. Schmidt, *Adv. Funct. Mater.*, 2003, **13**, 511.
11 D. C. Sayle, S. A. Maicaneanu and G. W. Watson, *J. Am. Chem. Soc.*, 2002, **124**, 11429.
12 Y. Takita, K. Sano, T. Muraya, H. Nishiguchi, N. Kawata, M. Ito, T. Akbay and T. Ishihara, *Appl. Catal., A.*, 1998, **170**, 23.
13 L. Malavasi, M. C. Mozzati, S. Polizzi, C. B. Azzoni and G. Flor, *Chem. Mater.*, 2003, **15**, 5036.
14 E. Beaurepaire, V. Buissette, M.-P. Sauviat, D. Giaume, K. Lahlil, A. Mercuri, D. Casanova, A. Huignard, J.-L. Martin, T. Gacoin, J.-P. Boilot and A. Alexandrou, *Nano Lett.*, 2004, **4**, 2079.
15 F. Meiser, C. Cortez and F. Caruso, *Angew. Chem., Int. Ed.*, 2004, **43**, 5954.
16 L. Yu, H. Song, S. Lu, Z. Liu, L. Yang and X. Kong, *J. Phys. Chem. B*, 2004, **108**, 16697.
17 C. Tang, Y. Bando, D. Golberg and R. Ma, *Angew. Chem., Int. Ed.*, 2005, **44**, 576.
18 H. Meyssamy, K. Riwotzki, A. Kornowski, S. Naused and M. Haase, *Adv. Mater.*, 1999, **11**, 840.
19 Y.-P. Fang, A.-W. Xu, R.-Q. Song, H.-X. Zhang, L.-P. You, J. C. Yu and H.-Q. Liu, *J. Am. Chem. Soc.*, 2003, **125**, 16025.
20 Y.-W. Zhang, Z.-G. Yan, L.-P. You, R. Si and C.-H. Yan, *Eur. J. Inorg. Chem.*, 2003, 4099.
21 Y.-P. Fang, A-W. Xu and W.-F. Dong, *Small*, 2005, **1**, 967.
22 M. Cao, C. Hu, Q. Wu, C. Guo, Y. Qi and E. Wang, *Nanotechnology*, 2005, **16**, 282.
23 W. Bu, Z. Hua, H. Chen and J. Shi, *J. Phys. Chem. B*, 2005, **109**, 14461.
24 R. F. Kubin and A. N. Fletcher, *J. Lumin.*, 1982, **27**, 455.
25 R. Kijkowska, E. Cholewka and B. Duszak, *J. Mater. Sci.*, 2003, **38**, 223.
26 S. Lucas, E. Champion, D. Bregiroux, D. Bernache-Assollant and F. Audubert, *J. Solid State Chem.*, 2004, **177**, 1302.

27 C. R. Patra, G. Alexandra, S. Patra, D. S. Jacob, A. Gedanken, A. Landau and Y. Gofer, *New J. Chem.*, 2005, **29**, 733.
28 T. T. Eighmy, E. L. Shaw, J. D. Eusden and C. A. Francis, *Surf. Sci. Spectra*, 1998, **5**, 122.
29 Z. A. Peng and X. Peng, *J. Am. Chem. Soc.*, 2001, **123**, 1389.
30 N. Kodama, M. Yamaga and B. Henderson, *J. Phys.: Condens. Matter*, 1996, **8**, 3505.
31 F. A. Kröger and J. Bakker, *Physica*, 1941, **VIII**, 628.
32 L. Yu, H. Song, Z. Liu, L. Yang, S. Lu and Z. Zheng, *J. Phys. Chem. B*, 2005, **109**, 11450.
33 V. Buissette, M. Moreau, T. Gacoin, J.-P. Boilot, J.-Y. Chane-Ching and T. L. Mercier, *Chem. Mater.*, 2004, **16**, 3767.
34 S. S. Brown, H.-J. Im, A. J. Rondinone and S. Dai, *J. Colloid Interface Sci.*, 2005, **292**, 127.
35 O. Lehmann, K. Kömpe and M. Haase, *J. Am. Chem. Soc.*, 2004, **126**, 14935.